ORIGINAL PAPER

The Role of the Transfer Layer on the Sliding Wear Behaviour of a Cu-15Ni-8Sn Alloy Under Different Loads

Daoxi Li[1,2] · Zhi Wang[1,2] · Chao Zhao[1,2] · Zongqiang Luo[1,2] · Weiwen Zhang[1,2]

Abstract

We studied the microstructure of the transfer layer and its effect on the wear mechanism and wear properties of an aged Cu-15Ni-8Sn alloy against 100Cr6 bearing steel during dry sliding by changing the applied load. The results indicate that the aged Cu-15Ni-8Sn alloy shows different wear behaviour and wear properties when the applied load changes; specifically, the average friction coefficient and specific wear rate decrease quickly with increasing applied load under steady wear conditions. The sample tested under a relatively high applied load showed the best wear performance because the oxide layer in the transfer layer. The main wear mechanisms were found to change with variation in the applied load. Metallic nanocrystalline particles and relatively ductile copper oxides promoted the formation of a thick and dense oxide layer. Changes in the thickness and morphology of the oxide layer under different loads can significantly affect the wear mechanisms.

Keywords Cu-15Ni-8Sn alloy · Dry sliding wear · Transfer layer · Oxide layer

1 Introduction

Cu-15Ni-8Sn alloys have been widely used as bearing materials under dry sliding owing to their positive tribological performance and good resistance to shock and impact, with applications in aircraft landing gear bushings or heavy-duty mechanical systems in the aerospace, automotive, oil or gas industries [1–4]. During dry sliding, the wear losses suffered by the Cu-15Ni-8Sn alloy should be sufficiently low; for example, it is vital to prevent formation of a gap between the cylinder liner and the piston ring for engine efficiency [5, 6].

A tribo transfer layer is commonly formed near the surface of Cu-15Ni-8Sn alloy during dry sliding and usually consists of three layers with a total thickness of less than 10 μm [7–10]: an oxide layer (OL), a mechanically mixed layer (MML) and a severely plastically deformed layer (SPDL). Amongst these layers, the OL is highly oxidized as

a result of in situ sintering of oxide particles and wear debris when a high temperature is induced during the friction process, and oxidation occurs between the substrate matrix alloy and oxygen in the air [11–13]. The SPDL experiences severe plastic deformation as a result of high shear force causing plastic deformation during the friction process, and the layer comprises elongated nanocrystallites [14]. In the SPDL, streamlined deformation characteristics are usually observed along the friction direction. The MML is a transition region between the OL and SPDL and consists of mechanically mixed multilayers [8, 9].

It is well known that transfer layers play an important role in the resistance of a material to friction and wear [6, 9, 15–20]. The OL adhering to the contact surface is found to provide protection as a solid lubricant and can reduce the wear rate [6, 9, 21, 22]. For example, Gee and Zaat proposed that a thin and continuous OL may reduce the wear rate caused by dry friction of leaded brass against steel [23]. The MML, containing continuous oxide layers and deformed metallic layers, is also believed to play an important role in the tribological behaviour of contact materials by reducing the friction and wear rate [8–10]. One possible reason for this behaviour is that the MML is intrinsically harder than the matrix material that supports it. For example, the oxide and metallic phases co-deform in the MML, leading to improved wear resistance in Fe-base alloys [21, 24]. The

✉ Weiwen Zhang
mewzhang@scut.edu.cn; wangzhi@scut.edu.cn

1 Guangdong Key Laboratory for Processing and Forming of Advanced Metallic Materials, South China University of Technology, Guangzhou 510640, China

2 National Engineering Research Center of Near-net-shape Forming for Metallic Materials, South China University of Technology, Guangzhou 510640, China

effect of SPDL is also beneficial for improving the wear properties due to the occurrence of strain hardening in the SPDL, which may lead to a higher hardness than that of the undeformed matrix alloy.

It is well known that wear mechanisms and their transitions are closely related to metallic matrix alloys and work conditions, such as applied load, sliding speed, friction medium and ambient temperature [25–27]. Especially during dry sliding, heat from friction can significantly affect tribological behaviour. The work condition consists of two important factors: applied load and sliding speed. For example, different amounts of friction heat can be released under different applied loads during sliding wear.

Although the effect of the whole transfer layer on the friction and wear rate has been well acknowledged, there is currently no clear understanding of the intrinsic relationship between the individual layer characteristics within the transfer layer and the wear resistance ability. However, the individual layers, such as the OL, MML and SPDL, can be changed significantly under different applied loads, which could in turn significantly affect the wear behaviour and wear mechanisms of the Cu-15Ni-8Sn alloy. Therefore, the present work focuses on the effect of various individual layer features on the specific wear rate and wear mechanisms of Cu-15Ni-8Sn alloys by changing the applied load during dry sliding.

2 Experimental Methods

In this study, the microstructure, mechanical properties and wear properties of a heat-treated (TX00) Cu-15Ni-8Sn-0.3Si-0.1Ti alloy (henceforth referred to as TX00 Cu-15Ni-8Sn) were studied. The alloy was melted in an intermediate-frequency induction furnace and then cast in a two-cavity steel mould with a diameter of 60 mm and a length of 160 mm. The chemical composition of the casted alloy was determined by spectrometry, and is the results are summarized in Table 1. The cast ingots were homogenized at 840 °C for 8 h and machined into cylindrical samples with dimensions of φ50 mm × 50 mm for extrusion. Hot extrusion was performed at 900 °C with an extrusion ratio of 17 and a ram speed of 3 mm/s and naturally cooled to room temperature in air. The as-extruded rods were subjected to solution treatment and ageing treatment in sequence with operation

Table 1 Chemical compositions of the TX00 Cu-15Ni-8Sn alloy (wt%)

Ni	Sn	Si	Ti	Cu
15.09	7.98	0.18	0.14	Balance

procedures of 820 °C × 1 h and 400 °C × 4 h, respectively, and both were quenched in water.

Wear tests of the TX00 Cu-15Ni-8Sn alloy were carried out using an MM-2000 block-on-ring tester under dry sliding at room temperature, with a speed of 400 r/min, a constant sliding time of 25 min and different applied loads of 100 N, 200 N, 300 N and 400 N. The schematic of the wear testing method is shown in Fig. 1. The aged alloy was machined to 10 mm × 10 mm × 10 mm for sliding as wear specimens. The wear specimens were ground using water abrasive paper from 400 to 3000 grits and then ultrasonically cleaned with ethyl alcohol for 15 min. The ageing specimens were treated against a ring composed of 100Cr6 (the hardness was 60 HRC) with an outer diameter of 45.25 mm, a width of 10 mm, and Ra0.4. The friction coefficient was continually recorded automatically by the wear tester during dry sliding. The average friction coefficient was calculated for each wear test within the steady-state regime (300–1500 s). The specific wear rate was calculated with the following equations:

$$w = \frac{\rho \times \Delta v}{2 \times \pi \times \omega \times t \times F} \tag{1}$$

$$\Delta v = \frac{\beta \times b^3}{12 \times r} \tag{2}$$

where w is the specific wear rate (g/Nm), Δv is the loss volume (mm³), ρ is the density (g/cm³), ω is the speed of the ring (r/min), t is the wear testing time (min), F is the applied load (N), β is the width of the counter ring (mm), b is the average width of the wear track on the block (mm), and r is the outer radius of the ring (mm). Wear tests under the same load were carried out five times to ensure repeatability, and the average result of the tests was reported.
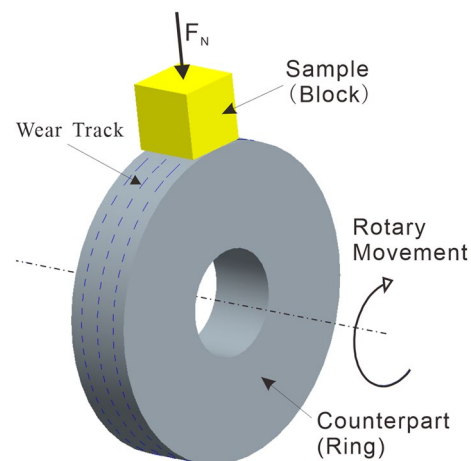

Fig. 1 Schematic of the block-on-ring testing method

The average size of the nanograins and the average thickness of the OL, MML, and SPDL were measured at more than 10 random areas of each sample from scanning electron microscopy (SEM) or transmission electron microscopy (TEM) images using Digital micrograph software. The morphologies of the TX00 Cu-15Ni-8Sn alloy were analysed by means of an FEI NONA430 scanning electron microscope in conjunction with electron backscatter diffraction (EBSD), energy dispersive X-ray spectrometry (EDS) and FEI Talos F200X transmission electron microscopy. The specimens used for SEM observation were prepared by polishing and then etching in a solution (5 g $FeCl_3$ + 10 mL HCl + 100 mL H_2O). Before the EBSD measurement, the samples were prepared by electropolishing using a solution of 50% phosphoric acid and 50% alcohol at 6.5 V for 60 s. The TEM samples were prepared by the twin-jet electropolishing method in 95% alcohol and 5% perchloric acid at − 20 °C. The TEM specimens of the cross section of the transfer layer for the sample after dry sliding were prepared by ion beam thinning (Gatan 695 ion beam thinner).

3 Results and Discussion

3.1 The Microstructure of the TX00 Cu-15Ni-8Sn Matrix Alloy

Figure 2 shows the microstructure of the TX00 Cu-15Ni-8Sn alloy as determined by SEM, EBSD, and high-resolution transmission electron microscopy (HRTEM). The alloy shows uniform fine equiaxed grains with an average size of 3.8 μm, as measured by EBSD. As shown in Fig. 2b, the matrix is a disordered face-centred cubic α phase (grey region), and γ-phase precipitates are located both in the interior grain and along the grain boundaries. The γ phase is found to be an ordered DO_3 phase [28, 29]. The matrix shows spinodal decomposition leading to the formation of small modulated structures of Sn-rich and Sn-lean zones. The light and dark contrast areas in Fig. 1c correspond to the modulated Sn-rich and Sn-lean regions, respectively, and are similar to reported works [8, 30]. DO_{22} and $L1_2$ diffraction spots were detected in the FFT pattern [29, 31], confirming the formation of ordered phases from the matrix (Fig. 2d).

3.2 Friction and Wear Properties

Figure 3 shows the typical friction coefficient curves of the TX00 Cu-15Ni-8Sn alloy mated with the 100Cr6 alloy as a function of sliding time under applied loads of 100–400 N during dry sliding. Figure 4 shows the summarized mean friction coefficient of the steady state of the samples tested under different loads. The friction coefficient for the samples tested under 400 N shows extremely irregular and large

fluctuations owing to the severe plastic deformation and decohesion of the tribo-layer, which can be proven by the worn surface observed later in this work. This fluctuation is beyond steady dry sliding, and therefore, in the following discussion, we will focus on the samples tested under suitable loading (100–300 N) without excessively large fluctuations. The friction coefficients-versus-time curves show similar characteristics for the tests under applied loads in the range of 100–300 N: a transient period, a relatively single steady-state regime, and finally, a relatively large fluctuation range of the friction coefficient. The transient period in the initial stage of dry sliding shows a larger friction coefficient when a low load is applied, which is a result of the contact of hard asperities on the worn surface and the interface of the grinding metal. During dry sliding, the worn surface becomes smooth, and thus, the friction coefficient remains at a relatively steady state. It is evident that the fluctuating intensity of the friction coefficient curves decreases as the load increases from 100 to 300 N (Fig. 3). When the applied load is 300 N, the friction coefficient reaches a steady state after a sliding time of approximately 300 s, and the average friction coefficient is 0.458. When the applied load is 100 N and 200 N, the average friction coefficients of the samples are 0.676 and 0.564, respectively.

Figure 5 shows the volume loss and specific wear rate of the TX00 Cu-15Ni-8Sn alloy mated with a 100Cr6 alloy under different applied loads. The volume loss increases with increasing load at loads below 200 N, and then it decreases to the minimum value of 3.8 mm^3 when the load increases to 300 N. With further increases of the load to 400 N, the volume loss increases significantly to 91 mm^3. It is known that the volume loss is not proportional to the normal load, indicating that the main wear mechanisms change when the load increases to the critical values. In addition, the specific wear rate shows a similar trend with increasing load. The samples tested under 100 N and 200 N show specific wear rates on the same order, with values of 2.82 and 2.32 × 10^{-7}, respectively. The sample tested under 300 N shows a minimum value of 8.0 × 10^{-8}. With a further increase in the load to 400 N, the specific wear rate increases significantly to 1.42 × 10^{-6}.

3.3 Worn Surfaces and Debris

Figure 6 shows the SEM micrographs of the worn surfaces, and Fig. 7 shows the collected wear debris under different applied loads. The samples under 100 N and 200 N show a considerable amount of granular wear debris adhered to the worn surface and continuous relatively deep grooves parallel to the sliding direction. The wear debris constitutes both large flakes and equiaxed particles. The worn surface and debris indicate that abrasive wear and adhesive wear simultaneously occurred during dry sliding under intermediate
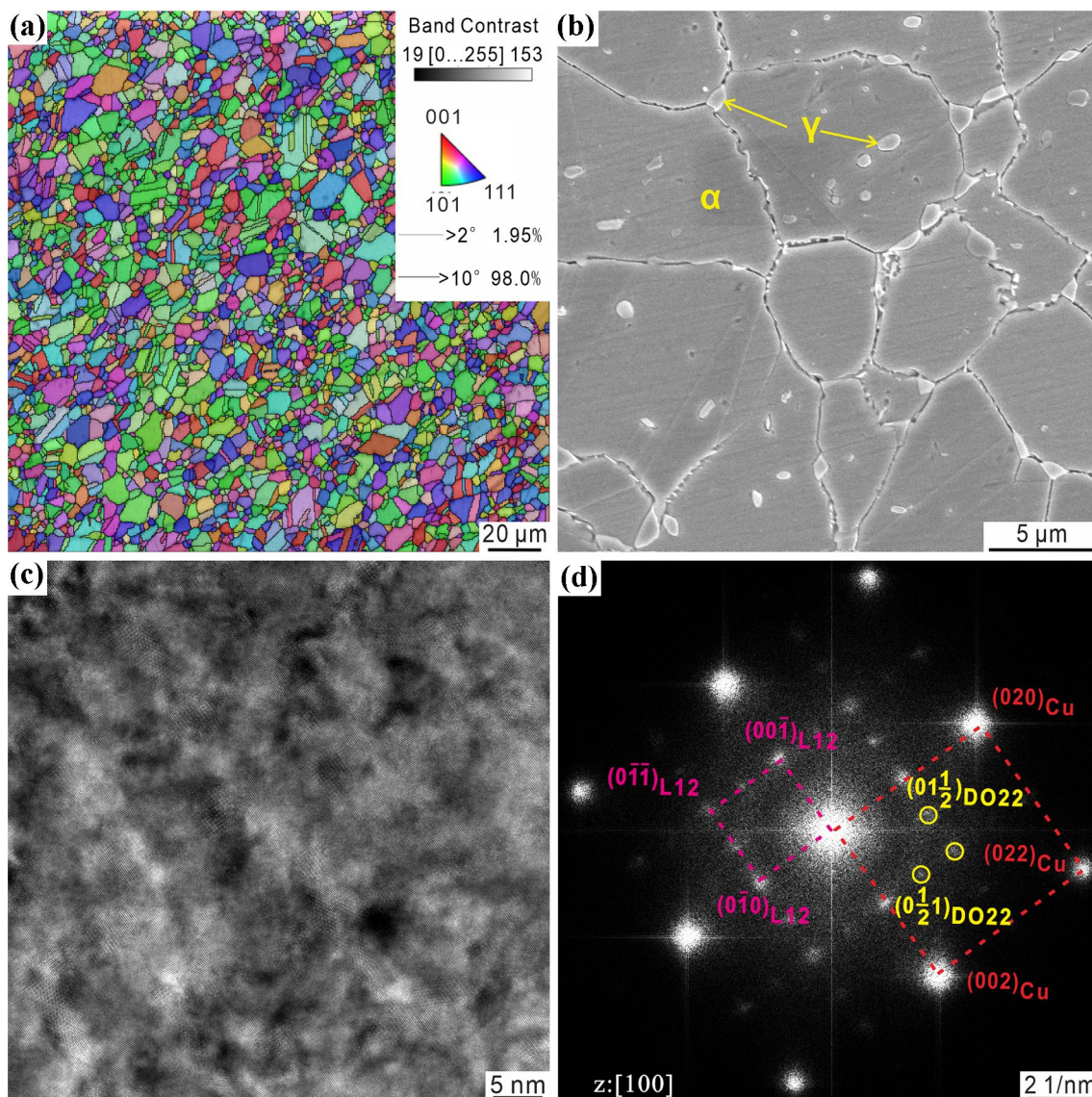
Fig. 2 Microstructure of the TX00 Cu-15Ni-8Sn alloy: **a** band contrast micrograph with inverse pole figure (IPF) colouring, **b** SEM micrograph, **c** HRTEM micrograph viewed along [100]$_{Cu}$, **d** fast Fourier transform (FFT) pattern of (**c**) along [100]$_{Cu}$

loads of 100 and 200 N. The samples under 300 N show a relatively smooth worn surface with a few fine particles and few shallow microploughs parallel to the sliding direction. The leading feature of the debris changes from large flakes to smaller equiaxed particles. The sample under 400 N shows deep subsurface cracks and large areas of peeling, where delamination of the material occurs as a result of severe plastic deformation. The debris is mostly extremely large blocks, which is consistent with subsurface decohesion leading to a sharp increase in the specific wear rate.

Table 2 shows the elemental analysis of Cu, Ni, Sn, Fe, and O for the worn surface and debris. The surface and debris are rich in oxygen, indicating that the worn surfaces are oxidized during dry sliding. The Fe content is as high

as 60 wt% in the debris, indicating a large content of iron oxide, which originated from the 100Cr6 alloy of the friction couple ring, and the O originated from air during the wear process. The sample under an applied load of 400 N shows high contents of matrix elements such as Cu, Ni, and Sn, which is a result of lower oxidation than the samples under an applied load of 300 N.

To help understand the wear behaviour, we chose wear debris from the samples under 300 N for TEM morphology observation, as these samples have the lowest specific wear rate, a steadier friction coefficient and a smaller fluctuation range. As shown in Fig. 8a and b, the wear debris was composed of equiaxed nanocrystallites. The diffraction patterns of the nanocrystallites reveal the existence of CuO, Cu_2O,
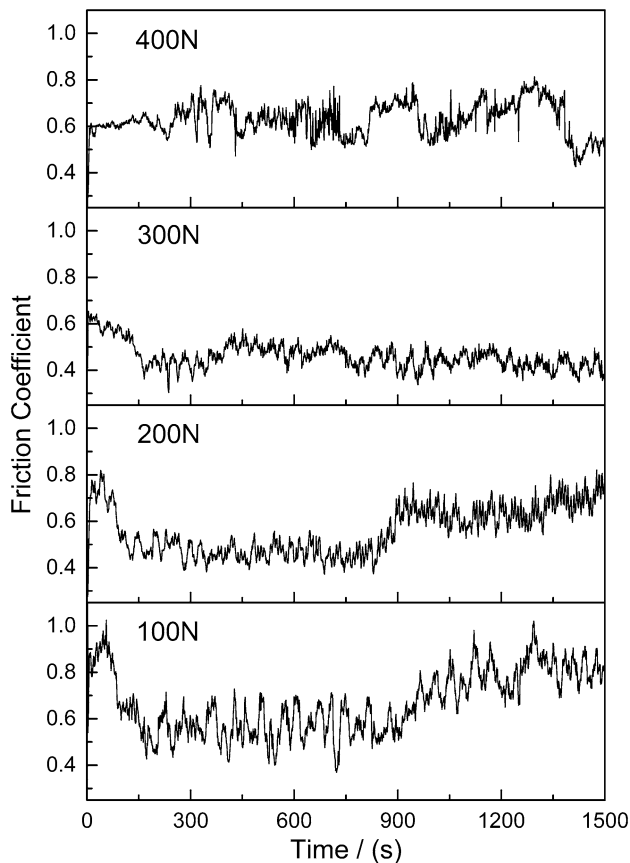
Fig. 3 Typical friction coefficient curves as a function of sliding time under different applied loads
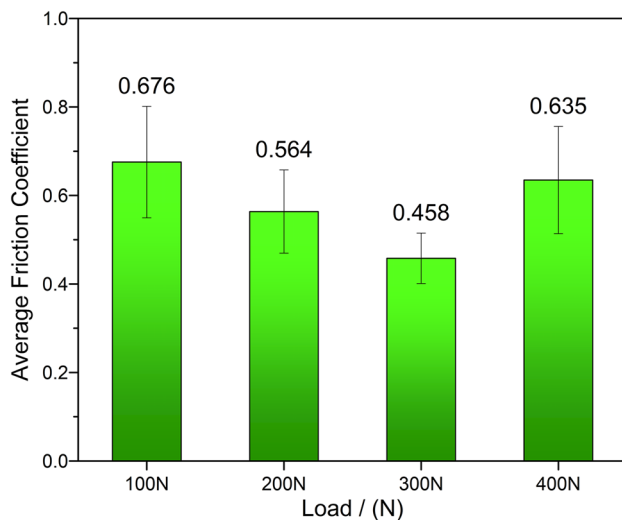

Fig. 4 Average friction coefficients under different applied loads

Fe_2O_3, the α matrix and the $CuNi_2Sn$ phase, as shown in Fig. 8c. The element distribution maps of the debris for the studied alloy under an applied load of 300 N are shown in

Fig. 8e - i. Fe, O, Cu, Ni, and Sn are uniformly intermixed and distributed, whilst Sn is very scarce. It should be emphasized that the oxide phases observed in this study are not pure. For example, the Fe_2O_3 phase is an $(Fe, Cr)_2O_3$ oxide [9]. Likewise, the CuO phase is a $(Cu, Ni, Sn)O$ oxide phase rather than pure CuO [32]. Therefore, it can be inferred that the fine debris of the alloy under an applied load of 300 N is composed of a metal oxide and TX00 Cu-15Ni-8Sn nanoparticles.

3.4 Characteristics of the Transfer Layer

Figure 9 shows the SEM images of the cross sections of the transfer layer of the TX00 Cu-15Ni-8Sn alloy under different applied loads, revealing multiple layers. From the top surface to the matrix, the subsurface can be divided into four regions: OL, MML, SPDL and matrix. The thicknesses of the OL, MML, and SPDL are different under various loads. At applied loads of 100 and 200 N, the OL has a characteristically very thin cross section (with a thickness less than 3 μm) and intermittent cracks. Interestingly, the sample under 300 N shows a much thicker OL (with a thickness of approximately 13 μm), which can be confirmed by the EDS element mapping shown in Fig. 10. The MML is a multi-lamellar structure with oxide layers and deformed metallic layers. The EDS element mapping shown in Fig. 10 confirms the overlapping of oxide layers and deformed metallic layers in the MML. In the SPDL, the grains are severely deformed and elongated along the sliding direction as a result of the high shear force during the friction process. For the sample under 400 N, some transverse cracks are observed, leading to transfer layer decohesion. This is consistent with the results of the worn surface and debris.

Table 3 shows the thickness of the OL, MML and SPDL for samples under different applied loads. The thickness of the OL, MML and SPDL changes with increasing applied load. The thickness of the OL increases significantly from ~ 1.7 μm under a load of 100 N to ~ 13.0 μm under a load of 300 N; the thickness of the MML remains relatively constant for the samples under loads of 100, 200, and 300 N; and the thickness of the SPDL increases with increasing applied load except at 400 N.

Figure 11 shows the TEM micrographs and EDS-STEM element mapping of the OL for the sample tested under 300 N, consisting of a mixture of a majority of oxide nanoparticles and a few metallic nanoparticles. The oxide nanoparticles are uniformly intermixed and distributed and are identified as Cu_2O, CuO, and Fe_2O_3 according to the selected-area diffraction patterns (SADP) shown in Fig. 11c. Fe_2O_3 particles are also observed, in which Fe originated from the counterpart 100Cr6 and O originated from the environment. The iron and copper oxide particles were mixed and transferred into the OL during dry sliding, showing
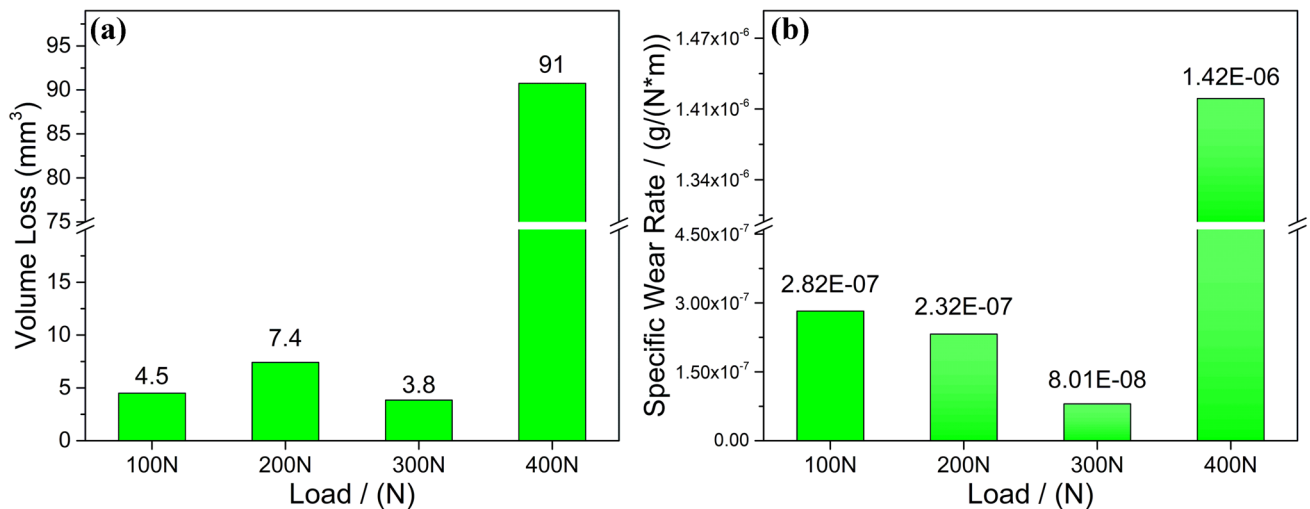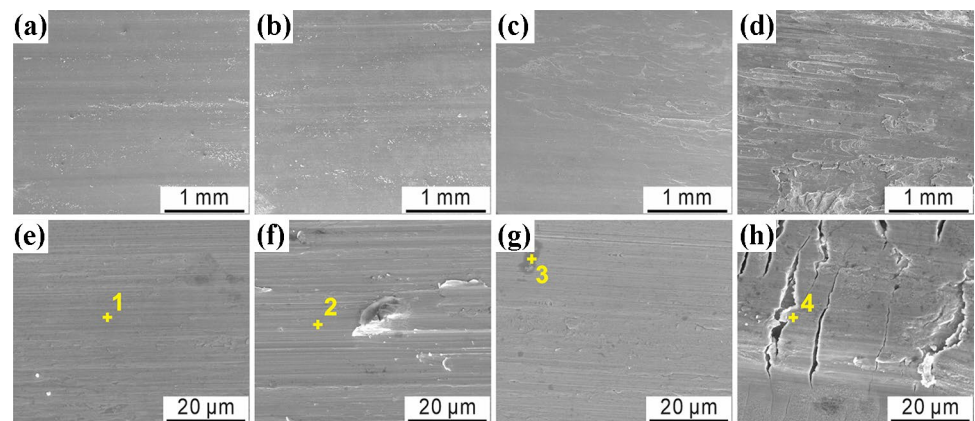
Fig. 5 Volume loss and average specific wear rate under different applied loads

Fig. 6 SEM micrographs of the worn surfaces after dry sliding at various applied loads: **a** and **e** 100 N; **b** and **f** 200 N; **c** and **g** 300 N; **d** and **h** 400 N

heavy oxidation where only sparkly copper-rich matrix nanograins can be found, as indicated by arrows in Fig. 11d.

As mentioned above, the MML is a transitional area with multilayer structures between the OL and SPDL, consisting of oxidation layers and deformed metallic layers. Figure 12 shows the EDS-STEM element mapping of a local area of the MML, revealing a sharp transition between the interface of the oxidation layer and the deformed metallic layer. The oxide layer in the MML consists mainly of iron oxides and has a small amount of copper oxides, similar to the OL. However, the oxide particles in the MML are much larger than those in the OL. Almost no O is observed in the deformed metallic layer, indicating less oxidation. Figure 13 shows the TEM micrographs of the deformed metallic layer in the MML, showing equiaxed nanograins with an average size of 55.3 nm. The primary phase is the α matrix, with a small amount of the secondary γ phase.

Figure 14 shows TEM micrographs of the top area of the SPDL close to the MML. The SADP from the SPDL shows a typical ring diffraction pattern corresponding to the nanocrystalline microstructure. The nanocrystalline particles are slightly elongated along the sliding direction owing to the shear force. The length and width of the nanocrystallites are approximately 415.6 and 92.1 nm, respectively. Figure 14d and e show the bottom area of the SPDL close to the matrix. Severe plastic deformation was observed, as evidenced by the highly curved and elongated grains. The size of the grains is much larger than that of the top SPDL. The dark areas in Fig. 14a, d, e, and f are regions with a high density of dislocations, as evidenced by the circled dark area in Fig. 14e showing highly stretched diffraction patterns and a high density of dislocations in the HRTEM micrograph of Fig. 14f. Figure 14 shows no evidence of oxidation of Fe, Cr and Cu in the SPDL.

4 Discussion

During the dry sliding of the TX00 Cu-15Ni-8Sn alloy against 100Cr6, significantly different wear behaviour and wear properties are observed when the applied load changes.

Fig. 7 SEM micrographs of the worn debris obtained at different applied loads: **a** 100 N, **b** 200 N, **c** 300 N, and **d** 400 N
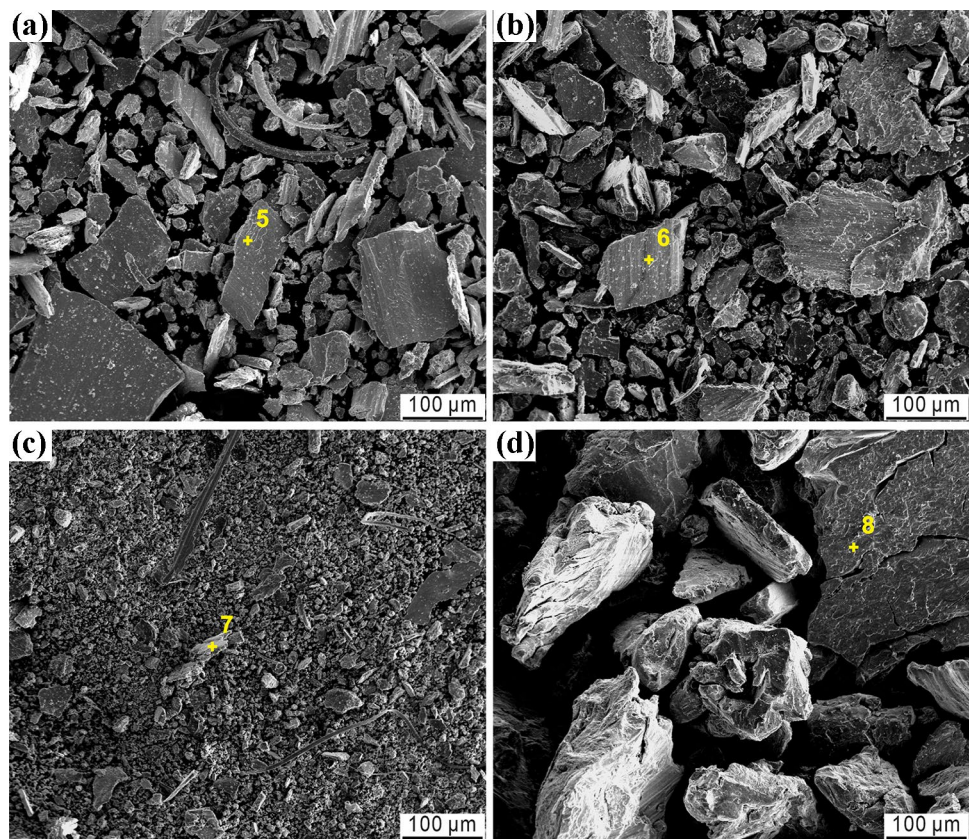

Table 2 EDS-SEM analysis results at the positions indicated in Figs. 5 and 6 (wt%)

Position	Cu	Ni	Sn	Fe	O
1 (Fig. 5e)	77.94	11.09	6.75	1.01	3.22
2 (Fig. 5f)	59.95	11.39	9.22	1.54	17.91
3 (Fig. 5g)	73.10	12.49	6.84	1.93	5.63
4 (Fig. 5h)	66.03	11.29	6.80	0.71	15.17
5 (Fig. 6a)	49.25	8.24	5.91	30.16	12.74
6 (Fig. 6b)	31.92	2.98	2.07	41.54	21.49
7 (Fig. 6c)	17.58	2.77	2.99	62.01	14.66
8 (Fig. 6d)	69.61	13.51	7.03	1.52	8.32

The average friction coefficients and the specific wear rate decrease quickly with increasing applied load under steady wear conditions. Furthermore, the friction coefficient curves indicate lower fluctuation at higher loads. This is different from most cases, in which the specific wear rate increases and becomes more unstable with increasing applied load during dry sliding. The unusual wear behaviour of the TX00 Cu-15Ni-8Sn alloy is closely related to the transfer layer and the mechanical properties of the metallic matrix. A leading changing feature of the transfer layer after dry sliding is that the thickness and morphology change significantly as the load increases, which plays a vital role in the wear behaviour. In this work, the metallic matrix is the same for the sliding wear tests; therefore, in the following discussion, we will focus on the effect of the transfer layer on the wear behaviour and wear properties under different applied loads.

The main wear mechanisms change with increasing applied load, which in turn significantly affects the wear properties, as mentioned above. For the sample tested under relatively low applied loads, such as 100–200 N, the wear mechanisms are mainly abrasive wear and adhesion wear, as seen by the worn surface and wear debris. A considerable amount of tiny granular wear debris adhering to the worn surface, many equiaxed debris particles and continuous relatively deep grooves parallel to the sliding direction indicate the occurrence of abrasive wear, whilst the large flake debris shows the simultaneous occurrence of adhesive wear. However, a relatively smooth worn surface is observed for the sample tested under an applied load of 300 N, indicating that the wear mechanisms change significantly when the abrasive wear and adhesive wear are drastically weakened. Furthermore, the debris changes from large flakes to smaller equiaxed oxide particles, revealing that oxidative wear, rather than abrasive wear and adhesive wear, prevails. For the sample under 400 N delamination, wear prevails at the sites of deep subsurface cracks and large areas of peeling of debris. With increasing applied load, the normal and tangential loads at the surface increase, leading to plastic
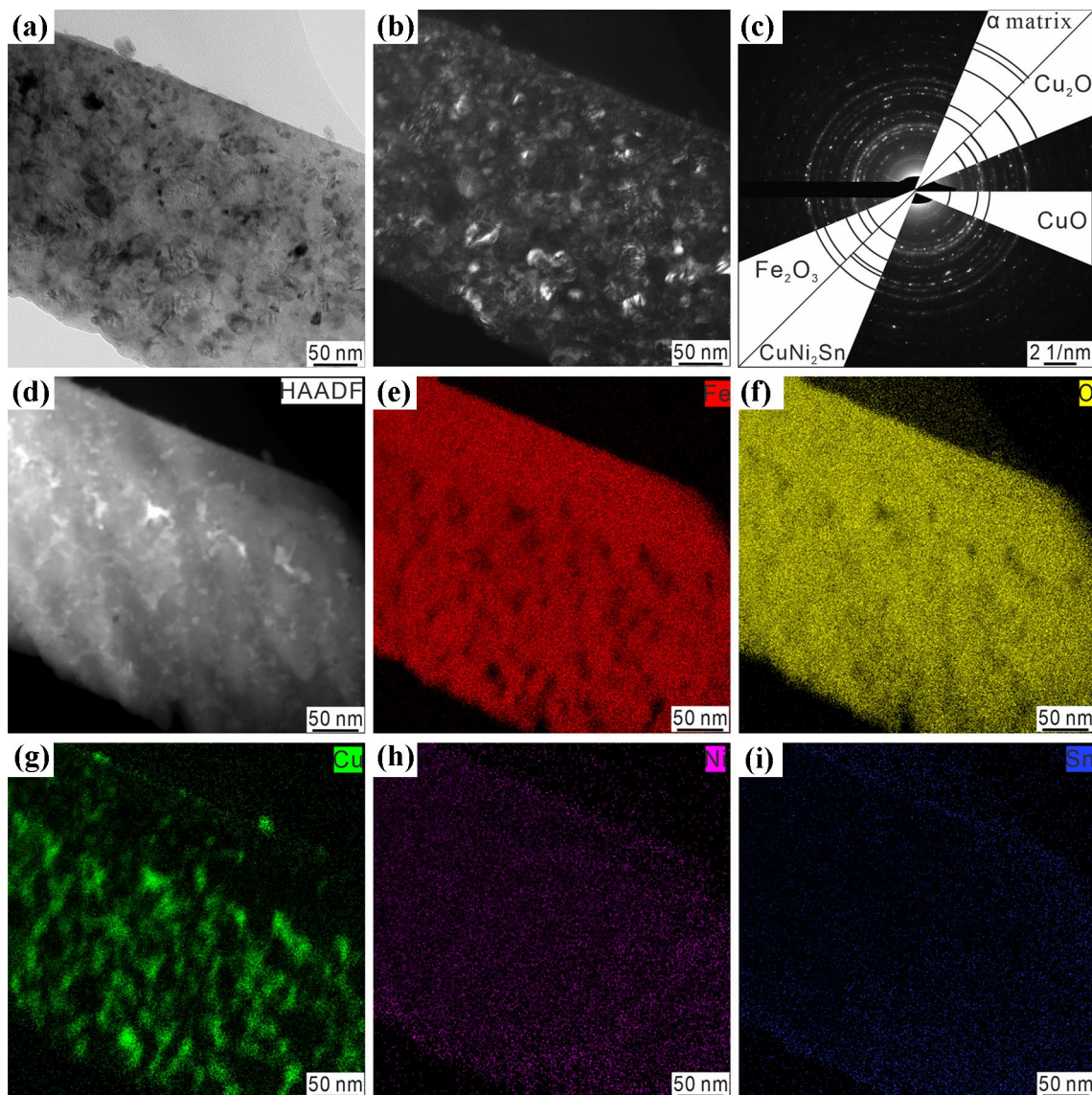
Fig. 8 TEM, SADP and EDS-TEM mapping of the TX00 Cu-15Ni-8Sn alloy under an applied load of 300 N. **a** Bright-field image, **b** dark-field image, **c** SADP of the debris, **d** HADDF image, and **e–i** EDS-TEM element distribution mapping images

shear deformation of the softer surface and accumulation with repeated loading action. Further loading and deformation cause the cracks to extend and propagate, joining neighbouring cracks. Finally, these cracks shear to the surface, causing delamination [33].

The wear mechanism transition is closely related to changes in the transfer layer. As mentioned above, the transfer layer can be divided into three regions: the OL, MML, and SPDL. One of the main changes is the thickness of the OL, which is significantly increased from ~1.7 μm under a load of 100 N to ~13.0 μm under a load of 300 N. This is beneficial for improving the wear resistance since a thick OL plays a protective role, leading to a small specific wear rate. This result is consistent with the lowest specific wear rate and steady friction behaviour of the results tested under 300 N.

The formation of a thick OL in the sample dry wear tested under 300 N can be attributed to the work condition and the large number of oxides as a result of the instant reaction between the surface of the metallic matrix and oxygen in the air, followed by in situ sintering of the oxide particles during sliding in the presence of friction heat and load. First, the higher load causes more heat and a higher pressure, which are helpful for pressing the oxide phases into thick layers. The transfer layer is believed to be constantly forming and breaking under steady-state conditions during the tribological process [8]. Second, the coarse grains in the metallic matrix are severely plastically deformed and transformed into equiaxed
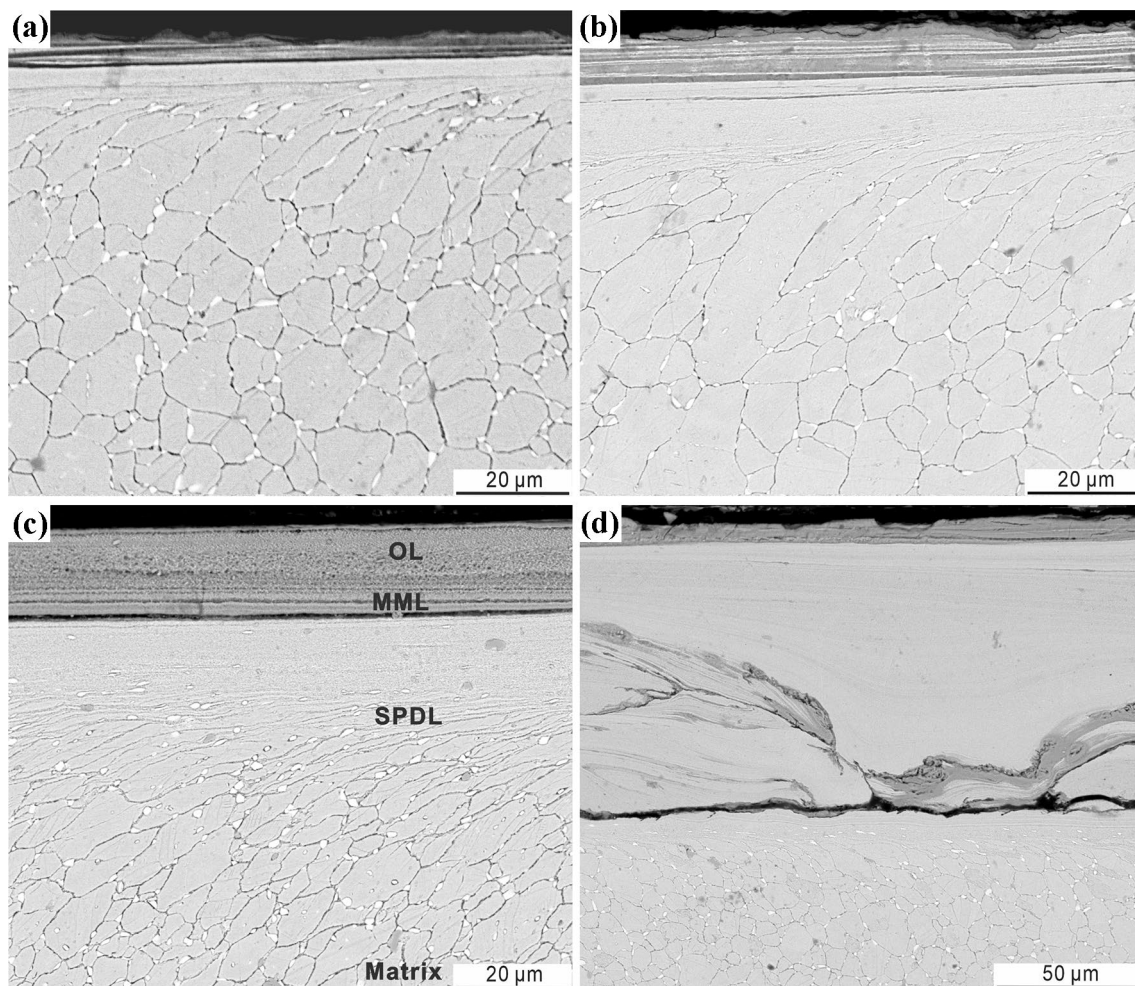
Fig. 9 SEM images of the cross sections of the TX00 Cu-15Ni-8Sn alloy under different applied loads: **a** 100 N, **b** 200 N, **c** 300 N, and **d** 400 N

nanocrystallites in the regions near the surface and the OL. Nanocrystallites with a high volume fraction of grain boundaries can promote oxidization and result in copper oxide nanoparticles. As shown in Figs. 10 and 11, the main phases are iron oxides, and many copper oxides are also homogenously distributed. Third, the copper oxides are relatively more ductile than the iron oxides, which is helpful for in situ sintering to form a thick and densified OL. It is well known that the OL can easily wear if the oxide film has too many brittle phases when the specific wear rate is greater than the oxidation rate; however, it is also possible to firmly bond to the metallic matrix if some relatively ductile oxide particles are included and distributed uniformly in the OL when the specific wear rate is less than the oxidation rate.

5 Conclusion

A detailed characteristic analysis of the transfer layer was conducted for an aged Cu-15Ni-8Sn alloy during dry sliding under different applied loads. The formation mechanisms of the transfer layer and its effect on the wear mechanism and wear properties were addressed. The following main conclusions were obtained:

1. The aged Cu-15Ni-8Sn alloy shows significantly different wear behaviour and wear properties when the applied load changes. The average friction coefficient and specific wear rate decrease quickly with increasing

Fig. 10 SEM images and the corresponding EDS-SEM mapping of the TX00 Cu-15Ni-8Sn alloy under an applied load of 300 N
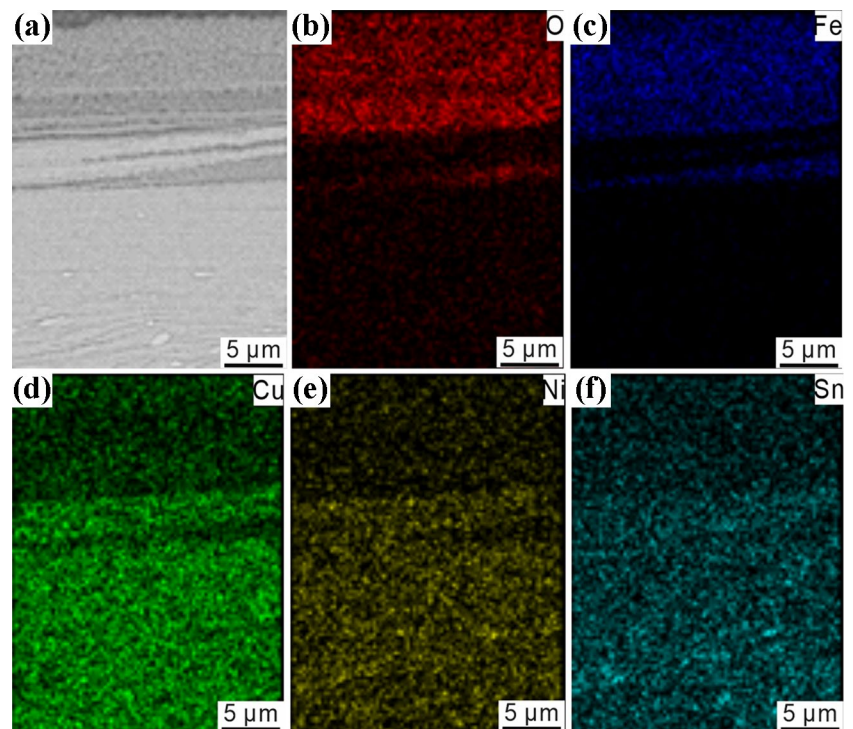
applied load except in the case of unstable sliding wear under a load of 400 N.

2. The thickness and morphology of the transfer layer change significantly as the load increases. The best wear performance of the sample tested under a relatively high applied load is mostly a result of the thickest OL layer, which plays a vital protective role during sliding wear.

3. The formation of a thick OL can be attributed to the work condition and the microstructure evolution. A higher load causes more heat and a higher pressure, which is helpful to increase the density and thickness of the oxide layer. The equiaxed nanocrystallites in the deformed regions near the OL promote oxidization and result in copper oxide nanoparticles. The copper oxides are relatively more ductile than the iron oxides, promoting in situ sintering to form a thick and dense OL.

4. The change in the thickness and morphology of the OL under different loads can affect the wear mechanism transition. The main wear mechanisms change with increasing applied load: abrasive wear and adhesion wear are the main wear mechanisms at low applied loads, oxidative wear prevails under relatively high applied loads, such as 300 N, and for the sample under 400 N, delamination wear predominates.
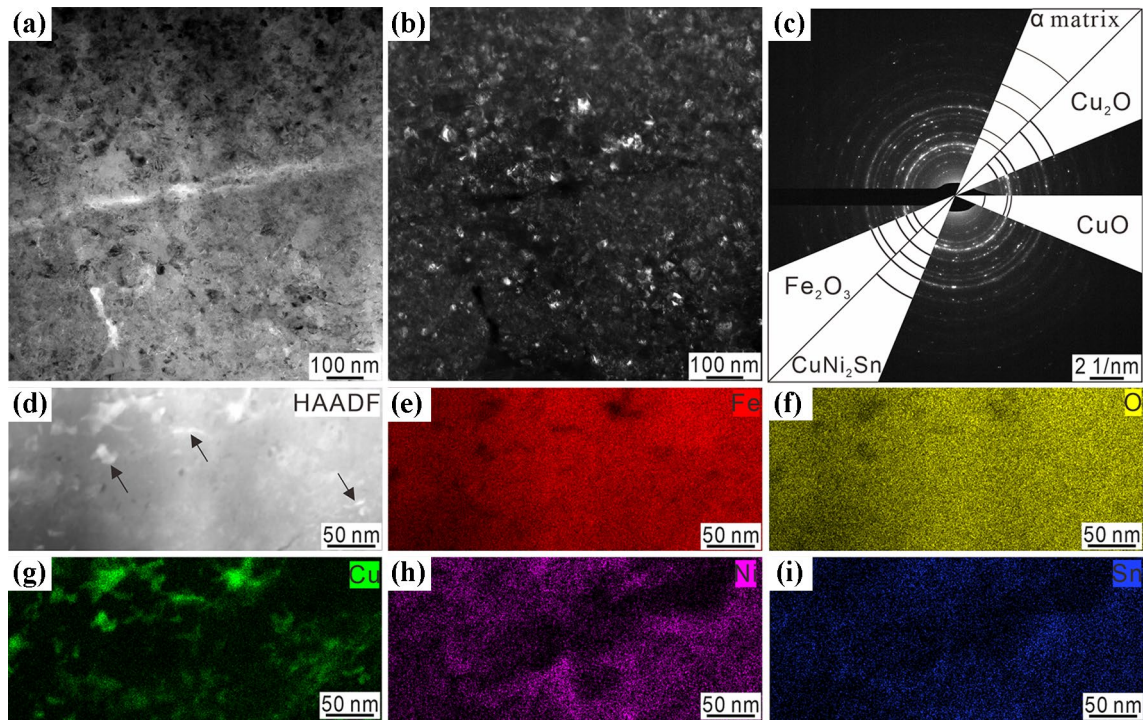
Table 3 Thickness of the OL, MML and SPDL for the samples under different applied loads

Load (N)	Thickness of the OL (μm)	Thickness of the MML (μm)	Thickness of the SPDL (μm)
100	1.63 ± 0.52	4.07 ± 0.72	29.02 ± 0.79
200	2.24 ± 0.59	9.48 ± 0.98	50.62 ± 0.69
300	12.97 ± 0.46	4.03 ± 0.62	64.68 ± 1.59
400	8.19 ± 1.59	94.36 ± 0.82	15.72 ± 1.60

Fig. 11 TEM analysis of the OL in the sample tested under an applied load of 300 N: **a** BF image; **b** DF image corresponding to (**a**); **c** SADP of the OL; **d** HAADF image, the arrows in (**d**) indicate metallic nanocrystalline particles, **e–i** EDS-STEM element mapping corresponding to (**d**)
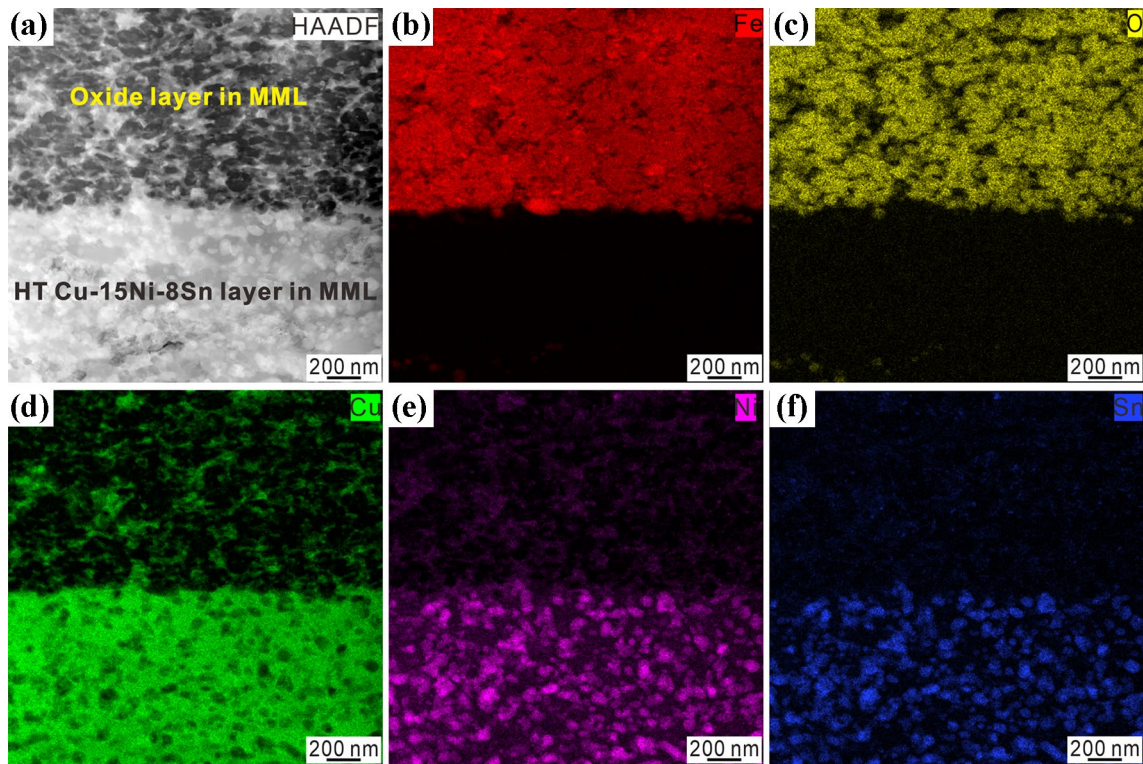

Fig. 12 Interface between the oxide layer and metallic layer in the MML: **a** HAADF and **b–f** EDS-STEM elemental mapping
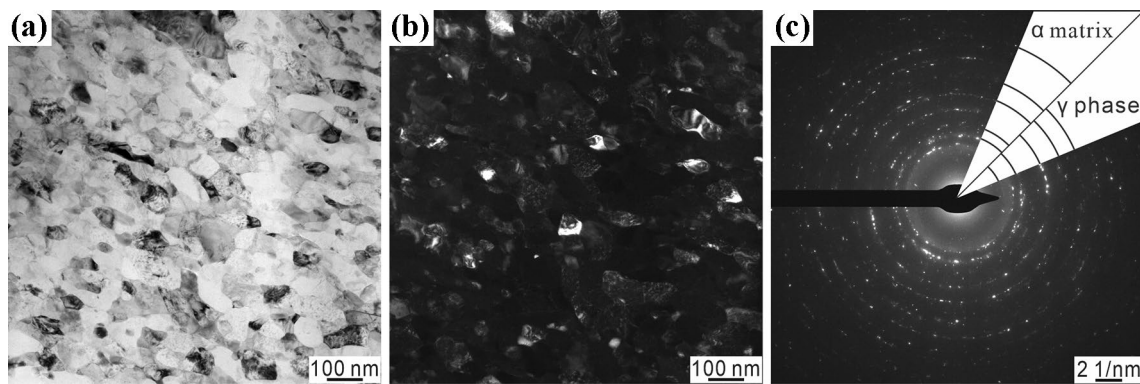
Fig. 13 The deformed matrix alloy layer in the MML: **a** BF image, **b** DF image corresponding to (**a**), **c** SADP of deformed matrix alloy layer in the MML
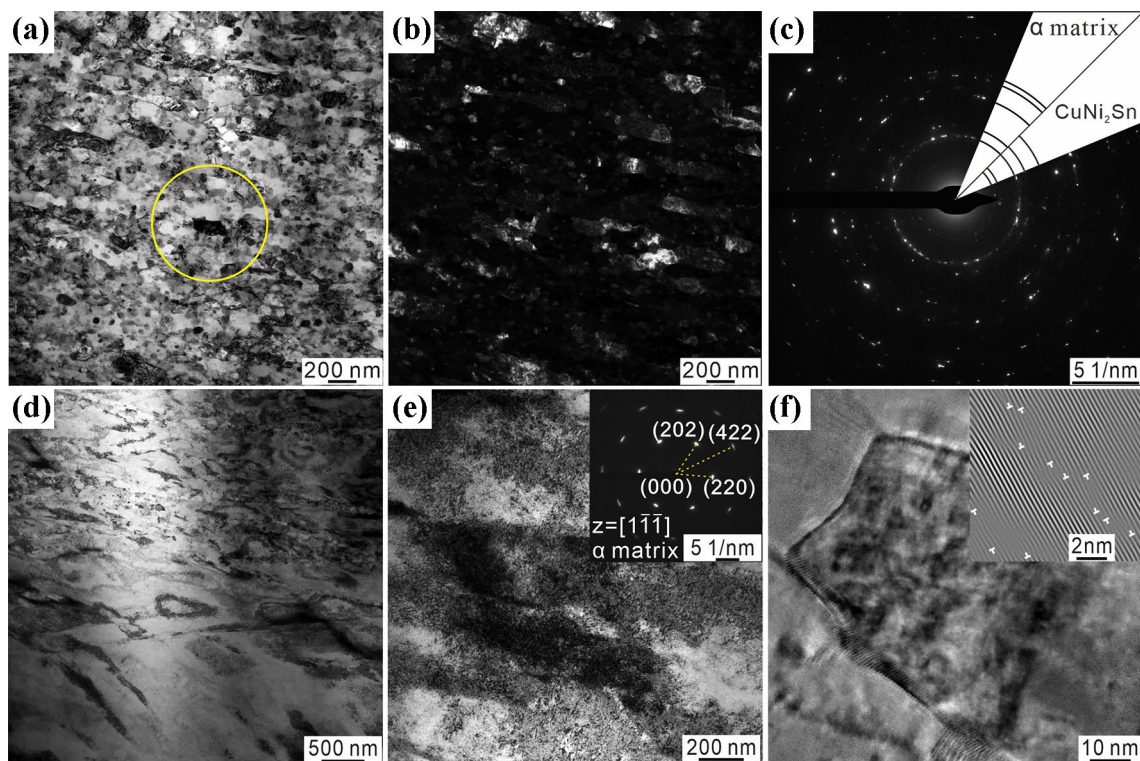

Fig. 14 TEM analysis of the SPDL. **a** BF image, **b** DF image corresponding to (**a**), **c** SADP of circled location in (**a**), **d** the SPDL near the matrix, **e** BF image and SADP of the SPDL near the matrix, and **f** HRTEM micrographs of the SPDL

Declarations

Conflict of interest The authors declare that they have no known competing financial interests or personal relationships that could have appeared to influence the work reported in this paper.

References

1. Cribb, W.R., Grensing, F.C.: Spinodal copper alloy C72900—new high strength antifriction alloy system. Can. Metall. Q. **50**, 232–239 (2011). https://doi.org/10.1179/1879139511Y.0000000012
2. Raymond Cribb, W., Ratka, J.O.: Copper spinodal alloys. Adv. Mater. Process. **160**, 1–4 (2002)
3. Raymond, W., Gedeon, M.J., Grensing, F.C.: Performance advances in copper-nickel-tin spinodal alloys. Adv. Mater. Process. **171**, 20–25 (2013)

4. Cribb, W.R.: Copper spinodal alloys for aerospace. Adv. Mater. Process. **6**, 44 (2006)

5. Deshpande, P., Dassenoy, F., Minfray, C., Jenei, I.Z., Le Mogne, T., Thiebaut, B.: Effect of adding TiO2 nanoparticles to a lubricant containing MoDTC on the tribological behavior of steel/steel contacts under boundary lubrication conditions. Tribol. Lett. **68**, 1–13 (2020). https://doi.org/10.1007/s11249-020-1278-0

6. Riahi, A.R., Alpas, A.T.: The role of tribo-layers on the sliding wear behavior of graphitic aluminum matrix composites. Wear **250–251**, 1396–1407 (2001). https://doi.org/10.1016/s0043-1648(01)00796-7

7. Zhu, J., Ma, L., Dwyer-Joyce, R.S.: Friction and wear of Cu-15 wt%Ni-8 wt%Sn bronze lubricated by grease at room and elevated temperature. Wear **460–461**, 203474 (2020). https://doi.org/10.1016/j.wear.2020.203474

8. Singh, J.B., Wen, J.G., Bellon, P.: Nanoscale characterization of the transfer layer formed during dry sliding of Cu-15 wt% Ni-8 wt% Sn bronze alloy. Acta Mater. **56**, 3053–3064 (2008). https://doi.org/10.1016/j.actamat.2008.02.040

9. Singh, J.B., Cai, W., Bellon, P.: Dry sliding of Cu-15 wt%Ni-8 wt%Sn bronze: Wear behaviour and microstructures. Wear **263**, 830–841 (2007). https://doi.org/10.1016/j.wear.2007.01.061

10. Feng, C., Wang, Y., Chen, W., Zhang, L., Zhou, K.: The mechanical mixed layer and its role in Cu-15Ni-8Sn/Graphite composites. Tribol. Trans. **60**, 135–145 (2017). https://doi.org/10.1080/10402004.2016.1152621

11. Lu, Z.C., Zeng, M.Q., Gao, Y., Zhu, M.: Minimizing tribolayer damage by strength-ductility matching in dual-scale structured Al-Sn alloys: a mechanism for improving wear performance. Wear **304**, 162–172 (2013). https://doi.org/10.1016/j.wear.2013.05.001

12. Kato, H., Komai, K.: Tribofilm formation and mild wear by tribo-sintering of nanometer-sized oxide particles on rubbing steel surfaces. Wear **262**, 36–41 (2007). https://doi.org/10.1016/j.wear.2006.03.046

13. Chandross, M., Argibay, N.: Friction of metals: a review of microstructural evolution and nanoscale phenomena in shearing contacts. Tribol. Lett. **69**, 1–27 (2021). https://doi.org/10.1007/s11249-021-01477-z

14. Wang, X., Wei, X., Zhang, J., Li, R., Hua, M., Wang, W.: Formation of nanocrystallized structure in worn surface layer of T10 steel against 20CrMnTi steel during dry rubbing. J. Nanomater. **2016**, 1 (2016). https://doi.org/10.1155/2016/4631851

15. Rigney, D.A.: Transfer, mixing and associated chemical and mechanical processes during the sliding of ductile materials. Wear **245**, 1–9 (2000). https://doi.org/10.1016/S0043-1648(00)00460-9

16. Cai, W., Bellon, P.: Subsurface microstructure evolution and deformation mechanism of Ag-Cu eutectic alloy after dry sliding wear. Wear **303**, 602–610 (2013). https://doi.org/10.1016/j.wear.2013.04.006

17. Chu, K., Ren, F., Zhu, W., Zhao, C., Bellon, P., Averback, R.S.: Sliding wear induced subsurface microstructural evolution in nanocrystalline Nb-Ag binary alloys and its impact on tribological performance. Wear **392–393**, 69–76 (2017). https://doi.org/10.1016/j.wear.2017.09.013

18. Li, X.Y., Tandon, K.N.: Mechanical mixing induced by sliding wear of an Al-Si alloy against M2 steel. Wear **225–229**, 640–648 (1999). https://doi.org/10.1016/S0043-1648(99)00021-6

19. Li, X.Y., Tandon, K.N.: Microstructural characterization of mechanically mixed layer and wear debris in sliding wear of an Al alloy and an Al based composite. Wear **245**, 148–161 (2000). https://doi.org/10.1016/S0043-1648(00)00475-0

20. Zhai, W., Sun, A., Zeng, W., Lu, W., Liu, X., Zhou, L., Wang, J., Mohamed, A., Ibrahim, M.: High wear resistance and mechanical performance of NiAl bronze developed by electron beam powder bed fusion. Tribol. Lett. **69**, 1–10 (2021). https://doi.org/10.1007/s11249-021-01534-7

21. Yin, C.H., Liang, Y.L., Liang, Y., Li, W., Yang, M.: Formation of a self-lubricating layer by oxidation and solid-state amorphization of nano-lamellar microstructures during dry sliding wear tests. Acta Mater. **166**, 208–220 (2019). https://doi.org/10.1016/j.actamat.2018.12.049

22. Cao, Y.G., Yin, C.H., Liang, Y.L., Tang, S.H.: Lowering the coefficient of martensite steel by forming a self-lubricating layer in dry sliding wear. Mater. Res. Express (2019). https://doi.org/10.1088/2053-1591/ab032a

23. Gee, A.W.J., Zaat, J.H.: Wear of copper alloys against oxygen and argon. Wear **5**, 257–274 (1962). https://doi.org/10.1016/0043-1648(62)90129-1

24. Yin, C.H., Liang, Y.L., Jiang, Y., Yang, M., Long, S.L.: Formation of nano-laminated structures in a dry sliding wear-induced layer under different wear mechanisms of 20CrNi2Mo steel. Appl. Surf. Sci. **423**, 305–313 (2017). https://doi.org/10.1016/j.apsusc.2017.06.187

25. Shen, M.X., Rong, K.J., Li, C.H., Xu, B., Xiong, G.Y., Zhang, R.H.: In situ friction-induced copper nanoparticles at the sliding interface between steel tribo-pairs and their tribological properties. Tribol. Lett. **68**, 1–11 (2020). https://doi.org/10.1007/s11249-020-01337-2

26. Ren, Q., Cui, G., Li, T., Hassani, M., Liu, Y., Kou, Z.: High-temperature wear behavior of cobalt matrix composites reinforced by LaF3 and CeO2. Tribol. Lett. **69**, 1–11 (2021). https://doi.org/10.1007/s11249-021-01524-9

27. Zhang, S.Z., Gan, X.P., Cheng, J.J., Jiang, Y.X., Li, Z., Zhou, K.C.: Effect of applied load on transition behavior of wear mechanism in Cu−15Ni−8Sn alloy under oil lubrication. J. Cent. South Univ. **24**, 1754–1761 (2017). https://doi.org/10.1007/s11771-017-3583-9

28. Zhao, C., Zhang, W., Wang, Z., Li, D., Luo, Z., Yang, C., Zhang, D.: Improving the mechanical properties of Cu-15Ni-8Sn alloys by addition of titanium. Materials **10**, 1–11 (2017). https://doi.org/10.3390/ma10091038

29. Zhao, J.C., Notis, M.R.: Spinodal decomposition, ordering transformation, and discontinuous precipitation in a Cu-15Ni-8Sn alloy. Acta Mater. **46**, 4203–4218 (1998). https://doi.org/10.1016/S1359-6454(98)00095-0

30. Wang, Y., Zhang, L., Xiao, J., Chen, W., Feng, C., Gan, X., Zhou, K.: The tribo-corrosion behavior of Cu-9 wt% Ni-6 wt% Sn alloy. Tribol. Int. **94**, 260–268 (2016). https://doi.org/10.1016/j.triboint.2015.06.031

31. Cheng, J.J., Gan, X.P., Li, Z., Lei, Q., Zhou, K.C.: Wear map for sliding wear behavior of Cu-15Ni-8Sn alloy against bearing steel under oil-lubricated condition. J. Cent. South Univ. **27**, 311–324 (2020). https://doi.org/10.1007/s11771-020-4297-y

32. Cheng, J., Gan, X., Lei, Q., Mao, M., Li, Z., Zhou, K.: Tribological behaviors of an ultrahigh wtrength Cu−15Ni−8Sn−0.2Y alloy sliding against TC6 titanium alloy in deionized water and seawater. Tribol. Lett. **68**, 1–18 (2020). https://doi.org/10.1007/s11249-019-1262-8

33. Suh, N.P.: An overview of the delamination theory of wear. Wear **44**, 1–16 (1977). https://doi.org/10.1016/0043-1648(77)90081-3